21cm Intensity Mapping + kSZ: for Larger Scale, Larger Area, Higher z Baryon Distributions

Dongzi Li,[1,2] Ue-Li Pen,[3,4,5,1] Hong-Ming Zhu,[6,7] and Yu Yu[8]

[1]*Perimeter Institute for Theoretical Physics, 31 Caroline St. N., Waterloo, ON, N2L 2Y5, Canada*
[2]*University of Waterloo, 200 University Ave W, Waterloo, ON, N2L 3G1, Canada*
[3]*Canadian Institute for Theoretical Astrophysics, 60 St. George Street, Toronto, Ontario M5S 3H8, Canada*
[4]*Dunlap Institute for Astronomy and Astrophysics, 50 St. George Street, Toronto, Ontario M5S 3H4, Canada*
[5]*Canadian Institute for Advanced Research, CIFAR Program in Gravitation and Cosmology, Toronto, Ontario M5G 1Z8, Canada*
[6]*Key Laboratory for Computational Astrophysics, National Astronomical Observatories, Chinese Academy of Sciences, 20A Datun Road, Beijing 100012, China*
[7]*University of Chinese Academy of Sciences, Beijing 100049, China*
[8]*Key laboratory for research in galaxies and cosmology, Shanghai Astronomical Observatory, Chinese Academy of Sciences, 80 Nandan Road, Shanghai 200030, China*

(Dated: December 9, 2016)

The prominent defficiency of baryon contents in observations for $z \lesssim 2$ and its close correlation with feedbacks and intergalactic medium conditions stand in the way of understanding structure evolution. To study the distribution of diffusive 'missing baryons', a large scale oriented probe, the kinematic Sunyaev-Zel'dovich (kSZ) effect on cosmic microwave background, was proposed. However, its faintness and lack of redshift require another signal to cross correlate with it. Previous proposals usually require galaxy spectroscopic surveys and new generation ground based CMB experiments to obtain convincing S/N. This induces constraints on redshift depth and sky coverage, and stops them to go below $l \sim 3000$ into larger scales. In this paper, a new possibility of cross correlating kSZ with HI density from 21cm intensity mapping is discussed. Ongoing intensity mapping experiments, eg. CHIME, making use of all weak sources, are able to cover large sky area and consistently measure $z \lesssim 2.5$ sky in next few years. This enable us to study structure evolution of $l \sim 1000 - 2000$, which is the scale of clusters and filaments. Taking into account of realistic constraints and using tidal signal to refine large scale informations, a minimum of 15 S/N for both redshift 1 and 2 could be reached with CHIME + Planck. The fast construction of interferometers with longer baselines, eg. HIRAX, may foster the S/N to reach 50 for redshift 2 with noise level of Planck.

PACS numbers:

I. INTRODUCTION

For $z \lesssim 2$, large fractions of predicted baryon contents are missing in observations. The majority of them are believed to reside in warm-hot intergalactic mediums (WHIM) with typical temperature of 10^5 K to 10^7 K [1, 2]. High temperature and low density in the medium, as well as uncertainties in ionization states and metalicities, make it difficult to derive information from metal absroption lines. It is expected urgently for probes that not only trace the majority of the baryons, but also can be interpreted model-independently.

Among proposed probes, the kinematic Sunyaev-Zel'dovich (kSZ) effect [3–5] is a promising one. kSZ effect results from Compton scattering of cosmic microwave background (CMB) off free electrons. The radial velocity of electrons will give photon a Doppler shift and hence leads to a secondary anisotropy in CMB temperature. It is an ideal probe to tackle the problem: First, it contributes from all the free electrons, indicating the distribution of 90% of the baryons in ionized states, leaving alone only less than 10% of baryons that reside in stars, remnants, atomic and molecular gases [6]. Second, the signal is mainly influenced by electron density and radial velocity, regardless the temperature, pressure and metalicity, so no extra assumptions are needed to estimate baryon abundance. Third, the peculiar velocity is dominantly related to large scale structures, therefore the signal is less biased towards local mass contraction, and more indicative about diffusive distributions.

Attractive as it is, two drawbacks largely reduce the feasibility of harnessing kSZ signal. First, the signal is weak and hence suffers seriously from contaminations from primary CMB, facility noises, thermal SZ effect, CMB lensing, etc. Second, it is an integrated effect along line of sight, therefore, kSZ itself does not contain redshift information.

A straight-forward mitigation of the disadvantages is to cross correlate kSZ signal with another tracer, which has both large scale structure and redshift information. Previous work has proposed optical spectroscopic survey as an ideal tool [7–9]. However, lack of prominent spectral lines at redshift $1.4 - 2.5$ make it difficult to consistently measure evolution from $z > 2$ to $z = 0$. Moreover, the high requirements on facility and sources largely constraint the sky coverage it could reach especially when redshift goes up, which limits it to only probe small angular scales, with primary CMB dies out. Methods trying to relax requirements on density fields, such as cross correlating photo-z galaxies with kSZ [10, 11], depend on models of velocity fields, demand next generation CMB facilities, eg. ACTpol, CMB-S4 to achieve convincing S/N.

In this paper, a new possibility of cross correlating HI density field from 21 cm intensity mapping to kSZ signal is discussed. HI 21 cm spectra have accurate redshift information, and are fully accessible for $z \lesssim 2$. Intensity mapping survey, rather than distinguishing individual galaxies, integrates all weak signals in a pixel, which enables it to reach high S/N and scan large sky area in much shorter time. In the following few years, there will be several experiments producing data of large sky area for redshift $\lesssim 2.5$ [12**?** , 13].

However, as feasibility is usually traded from data quality, there are three main challenges for the upcoming H I surveys in terms of cross correlation with kSZ. First, the integration of different signals will cause complicated foregrounds, which would smear the large scale structure in radial direction[14, 15]. Second, the angular resolution is also supressed by the integration, droping information of small scale structure in transverse plane. Third, till now, the proposed experiments all work on interferometers, which drain the largest scale structure on transverse plane due to the finite length of the shortest baseline.

On the other hand, the most prominate kSZ signals that could be distinguished from noises are mainly from $k_z \lesssim 0.1h/Mpc$ in radial direction with $l < 100$ and $l \sim 1000 - 2000$. These modes are partly damaged in intensity mapping due to the three challenges. In this paper, we evaluate the influence of the incompelete modes and partially recover the smeared large scale structures from their tidal influence on small scales[16, 17]. Final correlation is presented against different conditions.

The paper is organized as follows: In section II, we demonstrate given a density field, how to correlate it with kSZ signal in a holographic way similar to [8]. In section III, the weights of different Fourier modes on generating kSZ signals are discussed and used to evaluate existing modes in 21cm intensity mappings. In section IV, the method of 3D tidal reconstruction is introduced. Results of the reconstruction and cross correlation are presented in section V. And S/N is estimated via statistical error in section VI. Finally we conclude at section VII.

II. CROSS CORRELATE DENSITY FIELDS WITH KSZ MAP

The CMB temperature fluctuations caused by kSZ effect is simply an integral of the momentum field of free electrons:

$$\Theta_{kSZ}(\hat{n}) \equiv \frac{\Delta T_{kSZ}}{T_{\rm CMB}} = -\frac{1}{c}\int d\eta g(\eta) \boldsymbol{p}_{\parallel} \,, \tag{1}$$

where $\eta(z)$ is the comoving distance at redshift z, $g(\eta) = e^{-\tau} d\tau/d\eta$ is the visibility function, τ is the optical depth to Thomson scattering, $p_{\parallel} = (1+\delta_e)v_{\parallel}$ is the momentum field parallel to the line of sight, $\delta_e = (\rho - \bar{\rho})/\bar{\rho}$ is the electron overdensity, with $\bar{\rho}$ denotes the average density. It is assumed that electron overdensity are closely related to baryon overdensity δ at $z < 2$.

The direct correlation between kSZ and density field vanishes due to the cancellation of positive and negative velocity. To at most retrieve the correlation, we first linearly calculate the peculiar velocity fields $\boldsymbol{v_z}$ from continuity equation:

$$\hat{v}_z(\boldsymbol{k}) = iaHf\delta(\boldsymbol{k})\frac{k_z}{k^2} \tag{2}$$

where a is the scale factor, $f = d\ln D/d\ln a$, $D(a)$ is the linear growth function, H is the Hubble parameter.

We then reconstruct a 2D kSZ field with v_z and δ following Eq.(1), and quantify the tightness of correlation between

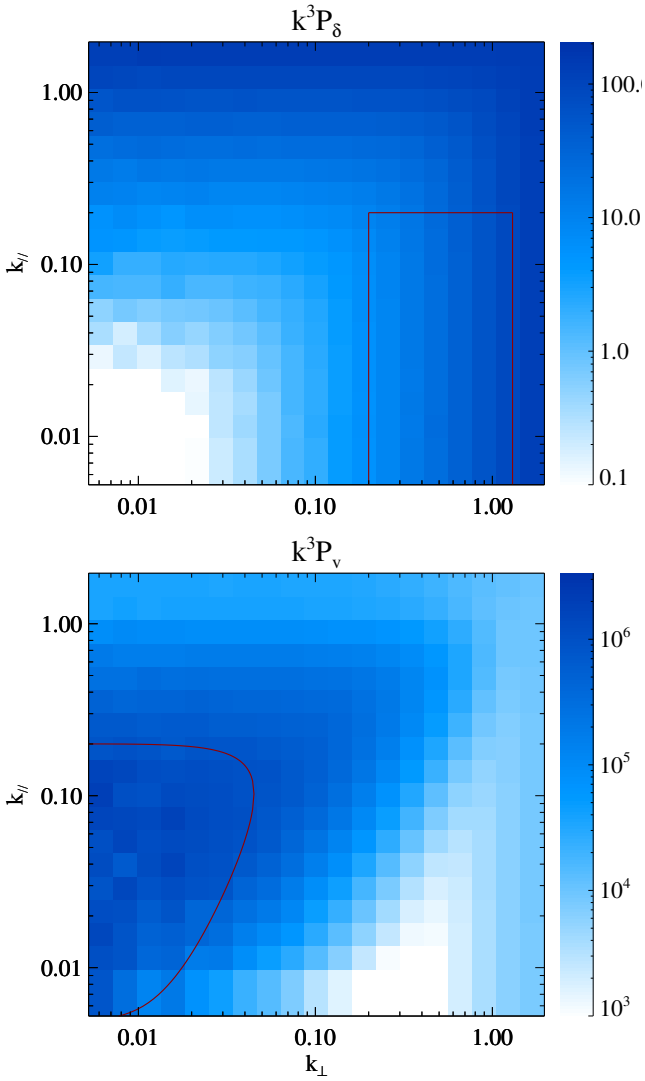

FIG. 1: Illustrating weights of different scales after integration. Demonstrated with data of redshift 1. (Top) The density variance $2\pi^2\Delta^2_\delta \equiv k^3 P_\delta$. (Bottom) The velocity variance $2\pi^2\Delta^2_{v_z} \equiv k^3 P_{v_z}$. (Red lines): Indicate most essential modes for generating kSZ signal in $\ell \sim 500 - 3000$.

reconstructed kSZ and real kSZ with a coefficient r:

$$r \equiv \frac{P_{recon,real}}{\sqrt{P_{recon}P_{real}}} \tag{3}$$

III. CHALLENGES FOR 21CM INTENSITY MAPPING

Ideally, this velocity reconstruction method should retrieve $> 90\%$ kSZ signals **??**. However, realistic 21cm intensity mapping experiments can only detect density fluctuations at certain scales, as illustrated in Fig.**??**. How much cross correlation we could construct is mainly affected by three conditions of the experiments:

1. The spacial and velocity resolution of facilities.

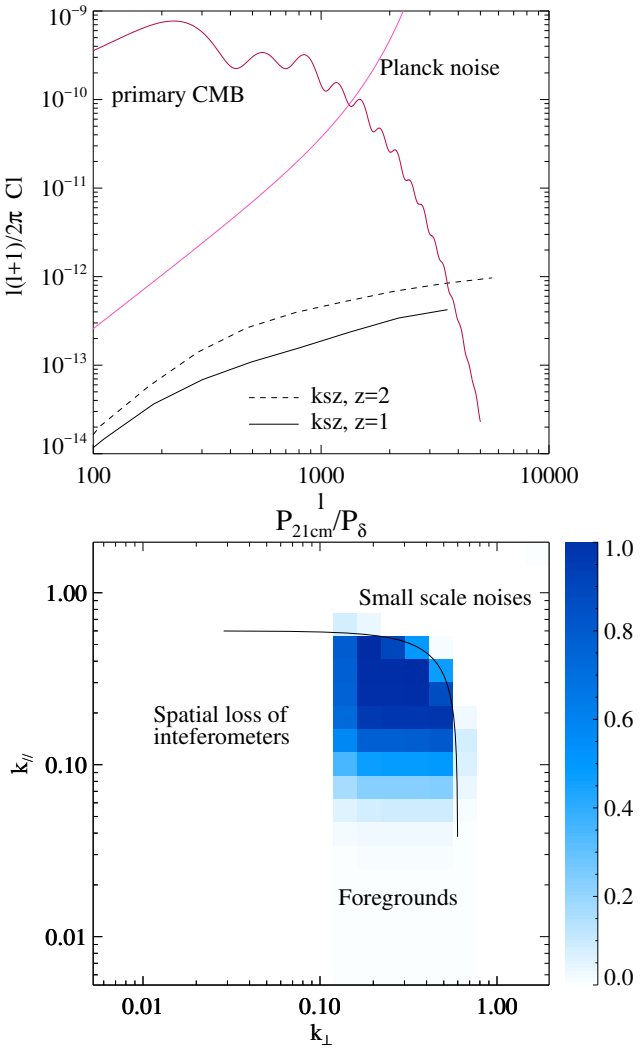

FIG. 2: (Top) Relative strength of angular powerspectrum between primary CMB, Planck noise in 217 GHz band, and kSZ effect in redshift 1 and 2. (Bottom) Available modes of density contrasts obtained in realistic 21cm Intensity Mapping experiments, with resolution of CHIME and high foregrounds ($R_\parallel = 15$ h/Mpc) in redshift 1. P_{21cm} is the remaining density powerspectrum after noise substraction; P_δ indicates the powerspectrum of a intact density field.

It decides the smallest scale to be observed, and the effect could roughly be resembled with a Heaviside Function $H(k_{\rm max} - k)$.

2. Foreground noise level:

Foregrounds from Galactic emissions, telescope noises, extragalactic radio sources and Radio recombination lines, could be three orders brighter than targeted signals[14, 15]. The process of foreground removal, taking advantage of its low spectral degrees of freedom [18], will inevitably contaminates the smooth large scale structure in radial direction. To imitate the loss, we apply a high pass filter $W(k_\parallel) = 1 - e^{-k_\parallel^2 R_\parallel^2/2}$.

3. The shortest baseline of inteferometers:

Current 21cm IM experiments are all carried on inteferometers. To avoid interactions, two beams of a interferometer cannot be placed infinitely close. The shortest baseline length decides the largest angular scale it could probe. Structures with angular scale greater than a threshhold of $l_{\rm min}$ will be drained out in the visibility function when cross correlating two beams. We again use a Heaviside function to assemble the effect.

	z=1		z=2	
	high foreground	low foreground	high foreground	low foreground
[a] $R_\parallel$ Mpc/h	15	60	10	40
	CHIME	HIRAX	CHIME	HIRAX
[b] $k_{\rm max}$ h/Mpc	0.6	1.2	0.4	0.8
[c] ℓ_{min}	300			

[a]Foreground: smear $k_z \lesssim 0.08, 0.02, 0.12, 0.03$ h/Mpc respectively. Parameters based on [19–21]

[b]Small scale noises: based on CHIME[22] and HIRAX[13] with 100 m and 200 m longest baseline respectively.

[c]Spatial loss of inteferomenter: assuming shortest baseline of 20 m.

TABLE I: Parameter of different noise filtering.

Therefore, a realistic 21 cm density contrasts will appear as

$$\delta_{\rm IM}(\boldsymbol{k}) = \delta(\boldsymbol{k}) H(k_{\rm max} - k) W(k_\parallel) H(l - l_{min}), \qquad (4)$$

Table.(I) lists several representive values for different parameters based on previous observations and predictions. Fig.**??** is a demonstration of density contrasts corresponding to $R_\parallel = 15$ Mpc/h, $k_{\rm max} = 0.6$ h/Mpc in $z = 1$.

Directly using $\delta_{\rm IM}$ of any of the parameters to reconstruct kSZ signal will yields a correlation coeffcient $r < 0.2$ with observable kSZ, indicating the loss of essential scales in kSZ generation.

IV. IMPORTANT SCALES FOR KSZ SIGNALS

We want to pinpoint the missing essential modes for generating kSZ signal.

The first step is to clarify which angular scale of the kSZ signal we look at. As demonstrated in Fig.**??**, the kSZ effect is too faint to be distinguished until primary CMB starts to fade away, which is roughly $\ell > 500$. It is possible to select a frequency band with thermal SZ signal negligible, then the dominate factor on high ℓ will be the CMB facility noises. Consider existing Planck [23] data at 217 GHz, $\ell \sim 500 - 3000$ will be the visible window for kSZ signal. The window could be extended to higher frequency with ACTpol and CMB-S4.

The next step is to understand what role each scale plays in generating kSZ signal at $\ell \sim 500 - 3000$. Write Eq.(1) in Fourier space. $\Theta(\boldsymbol{\ell})$ is propotional to the $k_z = 0$ mode of the momentum field, given $g(\eta)$ varies slowly.

$$\begin{aligned} \Theta(\boldsymbol{\ell}) &\propto p_\parallel(k_x\chi, k_y\chi, 0) \qquad (5) \\ &\propto \int d^3k'\, \delta(\boldsymbol{\ell}/\chi - \boldsymbol{k}'_\perp, k'_\parallel) v_z(\boldsymbol{k}') \end{aligned}$$

The convolution of δ and v_z indicates the signal comes from the cross talk of $\boldsymbol{\ell}/\chi - \boldsymbol{k}'_\perp$ and $\boldsymbol{k}_\perp$, sum over all $k\prime$.

Since $v_z \propto k_z/k^3$, it drops fast at small scales. Boldly analogize it to a Dirac delta function $\delta^D(\boldsymbol{k}\prime)$, $\Theta(\boldsymbol{\ell})$ will reduce to $\propto \delta(\boldsymbol{\ell}/\chi, 0)$. Although in reality, $v_z(\boldsymbol{k})$ wouldn't be as sharp as δ^D, and the peak will be more close to ($k_\perp$,$k_\parallel$)=(0.01,0.1) h/Mpc rather than (0,0), it is still safe to say that most of the kSZ signals are generated from the cross talk between a narrow box of k surrounding (0.01,0.1) h/Mpc for v_z and a narrow box of k close to $\delta(\boldsymbol{\ell}/\chi, 0.1)$ h/Mpc for δ.

The strenth of $|\delta(k)|$ and $|v_z(k)|$, as well as the important modes for each fields are indicated in Fig.1. Comparing it with Fig.**??**, we notice that while the essential modes for δ are partly resolved, the large scale information dominating v_z is almost completely drained out in 21 IM fields.

Therefore, the primary task to restore the cross correlation between kSZ and 21cm IM fields is to reconstruct the large scale modes for v_z.

V. COSMIC TIDAL RECONSTRUCTION

Till now only linear theories are considered in reconstruction, however, to extract the lost large scale information, we need to consider couplings between different scales in nonlinear theories. While there are a great variety of nonlinear effects, identifying a single one will help conduct clean reconstruction. Here, we present an algorithm to employ tidal coupling to solve for large scale structures [16, 17].

The evolution of small scale structure is modulated by large scale tidal force. We can select this effect and solve for the large scale potential.

Consider only the anisotropic influence from tidal force, the distortions on power spectrum can linearly be calculated as

$$\delta P(\boldsymbol{k},\tau)|_{t_{ij}} \;=\; \hat{k}^i\hat{k}^j t_{ij}^{(0)} P_{1s}(k,\tau) f(k,\tau) \qquad (6)$$

where f is the linear coupling function; $P_{1s}(k,\tau)$ is the theoretical small scale linear powerspectrum; and $\delta P(\boldsymbol{k},\tau)$ is the real distortion from observations.

We can solve for the unknown quantity t_{ij}, which is the tidal force tensor defined as

$$t_{ij} = \Phi_{L,ij} - \nabla^2\Phi_L\delta^D_{ij}/3 \qquad (7)$$

$\Phi_{L,ij}$ is the second derivative of large scale potential, and i,j indicates $\hat{x}, \hat{y}, \hat{z}$ directions, δ^D is the Dirac function.

With t_{ij}, we calculate the variance of large scale potential Φ_L and get the large scale density contrast $\kappa_{3\mathrm{D}}$.

$$\kappa_{3\mathrm{D}} \sim \nabla^2\Phi_L = \frac{3}{2}\nabla^{-2}\partial_i\partial_j t_{ij} \qquad (8)$$

Since $f(k,\tau)$ increase with k in our interested scales, the distortions are more obvious in small scales. Therefore, the method mainly use the quadratic statistics on small scales to recover the large scale density field. It works best for close linear regions.

Programming steps:

(1) Gaussianize the field, taking $\delta_g = \ln(1+\delta)$. This is to allieviate the problem that filter W_i in Eq.(11) heavily weights high density regions.

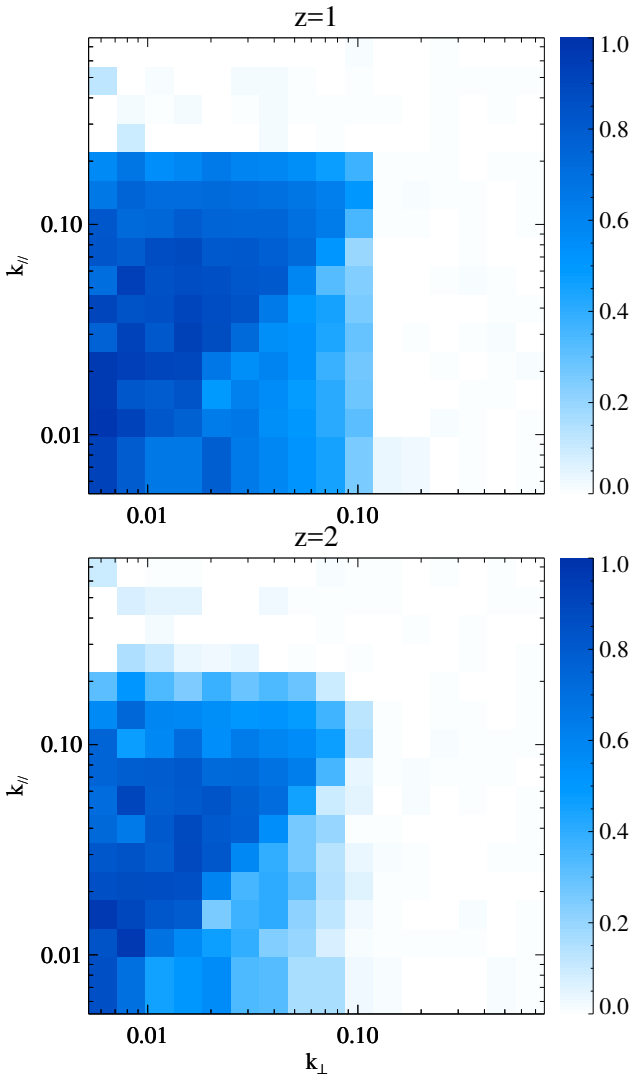

FIG. 3: Correlation coefficient r between reconstructed velocity field and real velocity field, assuming a baseline of 100m and serious foregrounds smearing k_z below 0.08 h/Mpc and 0.12 h/Mpc of redshift 1 and 2 respectively.

(2) Following gravitational lensing procedures, decompose the symmetric, traceless tidal force tensor into 5 components,

$$t_{ij} = \begin{pmatrix} \gamma_1 - \gamma_z & \gamma_\times & \gamma_2 \\ \gamma_\times & -\gamma_1 - \gamma_z & \gamma_y \\ \gamma_2 & \gamma_y & 2\gamma_z \end{pmatrix}. \qquad (9)$$

(3) Select density distortions caused by tidal force, by convolving δ_g with a filter W_i deduced from Eq.(6)

$$\delta_g^{w_i}(\boldsymbol{k}) = W_i(\boldsymbol{k})\delta_g(\boldsymbol{k}) \qquad (10)$$

$$W_i(\boldsymbol{k}) = i\left[\frac{P(k)f(k)}{P^2_{tot}(k)}\right]^{\frac{1}{2}}\frac{k_i}{k} = S(k)\frac{k_i}{k}$$

$f(k) = 2\alpha(\tau) - \beta(\tau)d\ln P/d\ln k$ is again the coupling function, with α and β related to linear growth funcion [17], and

calculated to be (0.6, 1.3) for $z = 1$ and (0.4, 0.9) for $z = 2$. $P_{tot} = P + P_{noise}$ is the observed matter powerspectrum, and P is theoretical matter powerspectrum,

(4) Estimate the 5 tidal tensor components from quadratic statistics.

$$\begin{aligned}
\hat{\gamma}_1(\boldsymbol{x}) &= [\delta_g^{w_1}(\boldsymbol{x})\delta_g^{w_1}(\boldsymbol{x}) - \delta_g^{w_2}(\boldsymbol{x})\delta_g^{w_2}(\boldsymbol{x})], \\
\hat{\gamma}_2(\boldsymbol{x}) &= [2\delta_g^{w_1}(\boldsymbol{x})\delta_g^{w_2}(\boldsymbol{x})], \\
\hat{\gamma}_x(\boldsymbol{x}) &= [2\delta_g^{w_1}(\boldsymbol{x})\delta_g^{w_3}(\boldsymbol{x})], \\
\hat{\gamma}_y(\boldsymbol{x}) &= [2\delta_g^{w_2}(\boldsymbol{x})\delta_g^{w_3}(\boldsymbol{x})], \\
\hat{\gamma}_z(\boldsymbol{x}) &= \frac{1}{3}[(2\delta_g^{w_3}(\boldsymbol{x})\delta_g^{w_3}(\boldsymbol{x}) \\
&\quad -\delta_g^{w_1}(\boldsymbol{x})\delta_g^{w_1}(\boldsymbol{x}) - \delta_g^{w_2}(\boldsymbol{x})\delta_g^{w_2}(\boldsymbol{x}))],
\end{aligned} \tag{11}$$

(5) Reconstruct large scale density contrast $\kappa_{3\mathrm{D}}$ from tidal tensor:

$$\begin{aligned}
\kappa_{3\mathrm{D}}(\boldsymbol{k}) = \frac{1}{k^2} \quad & [(k_1^2 - k_2^2)\gamma_1(\boldsymbol{k}) + 2k_1k_2\gamma_2(\boldsymbol{k}) \\
& +2k_1k_3\gamma_x(\boldsymbol{k}) + 2k_2k_3\gamma_y(\boldsymbol{k}) \\
& +(2k_3^2 - k_1^2 - k_1^2)\gamma_z(\boldsymbol{k})].
\end{aligned} \tag{12}$$

(6) Correct bias and suppress noise with a Wiener filter.

Due to the foregrounds, the noise in z direction will be different from x,y direction, therefore we apply an anisotropic Wiener filter.

$$\hat{\kappa}_c(\boldsymbol{k}) = \frac{\kappa_{3\mathrm{D}}(\boldsymbol{k})}{b(k_\perp, k_\parallel)} W(k_\perp, k_\parallel)\ , \tag{13}$$

Bias $b(k_\perp, k_\parallel) = P_{\mathrm{k3D},\delta}/P_\delta$ is the cross powerspectra between reconstructed field κ3D and original field δ, Wiener filter $W(k_\perp, k_\parallel) = P_\delta/(P_{\mathrm{k3D}}/b^2)$.

Here $\hat{\kappa}_c$ is the output large scale density contrast we obtain from tidal reconstruction. We use it to calculate velocity $\hat{v}_z^{\mathrm{tide}}$.

VI. SIMULATIONS AND RESULTS

To test the algorithm, six N-body simulations are performed with the CUBEP^{3}M code [24], each evolving 1024^3 particles in a $(1.2\mathrm{Gpc}/h)^3$ box. Simulation parameters are set as: Hubble parameter $h = 0.678$, baryon density $\Omega_b = 0.049$, dark matter density $\Omega_c = 0.259$, amplitude of primordial curvature power spectrum $A_s = 2.139 \times 10^{-9}$ at $k_0 = 0.05$ Mpc^{-1} and scalar spectral index $n_s = 0.968$.

Simulated density and velocity fields at $z = 1, 2$ are output and used to generate kSZ signal.

To avoid manipulating noises, we perform tidal reconstruction on most conservative estimates, i.e. $R_\parallel = 15$ Mpc/h, $k_{max} = 0.6$ h/Mpc, $\ell_{max} = 100$ for $z = 1$; and $R_\parallel = 10$ Mpc/h, $k_{max} = 0.4$ h/Mpc, $\ell_{max} = 100$ for $z = 2$.

The cross correlation between $\hat{v}_z^{tide}$ and v_z are demonstrated in Fig.3. Important modes for velocity fields (within redline of Fig.1 lower label) are well extracted with correlations greater than 0.7. The reconstruction on $z = 2$ is slightly worse than $z = 1$ due to stronger foreground and lower resolution.

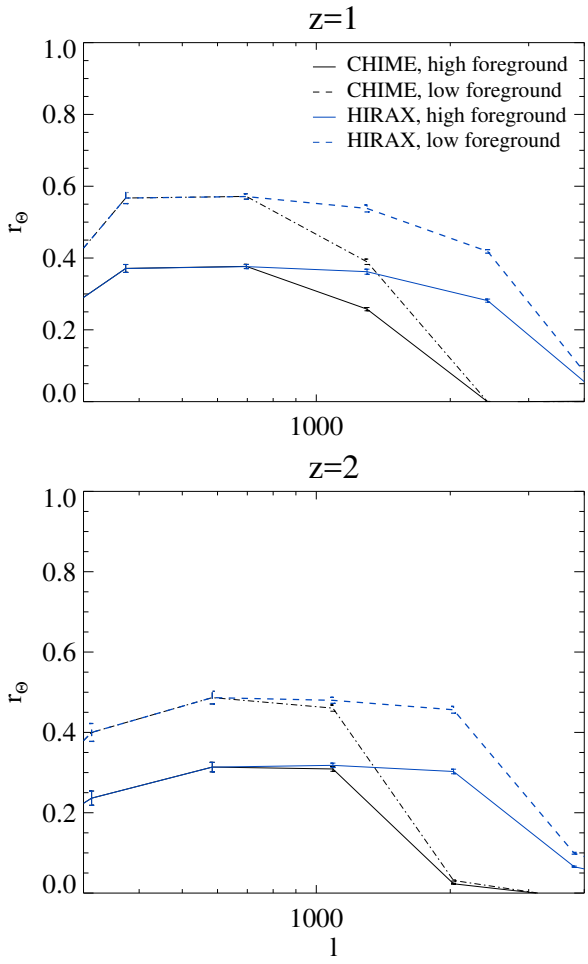

FIG. 4: The correlation coefficient r between real kSZ $P_{\Theta_{kSZ}}$ and reconstructed kSZ $P_{\hat{\Theta}_{kSZ}}$.

Combining reconstructed velocity field with density fields of different conditions, we get mock kSZ signals. Their correlation coefficients with exact kSZ are demonstrated in Fig.4. Even with identical tidal reconstructed velocity field, better foreground techneque can improve the correlation coefficient by 0.2. If the foreground is removed clean enough for more modes to be used in tidal reconstruction procedure, the improvement will be more notable. Resolution of facility will improve the reconstruction on higher ℓ, consisting with previous analysis.

VII. STATISTICAL ERROR AND S/N

Taking into account primary CMB and facility noises, the chance to seperate kSZ signal from statistical errors could be estimated as:

$$\begin{aligned}
\frac{S}{N} &= \frac{C_l}{\Delta C_l} \\
&\simeq r\sqrt{(2\ell+1)\Delta l f_{\mathrm{sky}}}\sqrt{\frac{C_l^{\mathrm{kSZ},\Delta z}}{C_l^{\mathrm{CMB}} + C_l^{\mathrm{kSZ}} + C_l^{\mathrm{CMB},N}}}
\end{aligned} \tag{14}$$

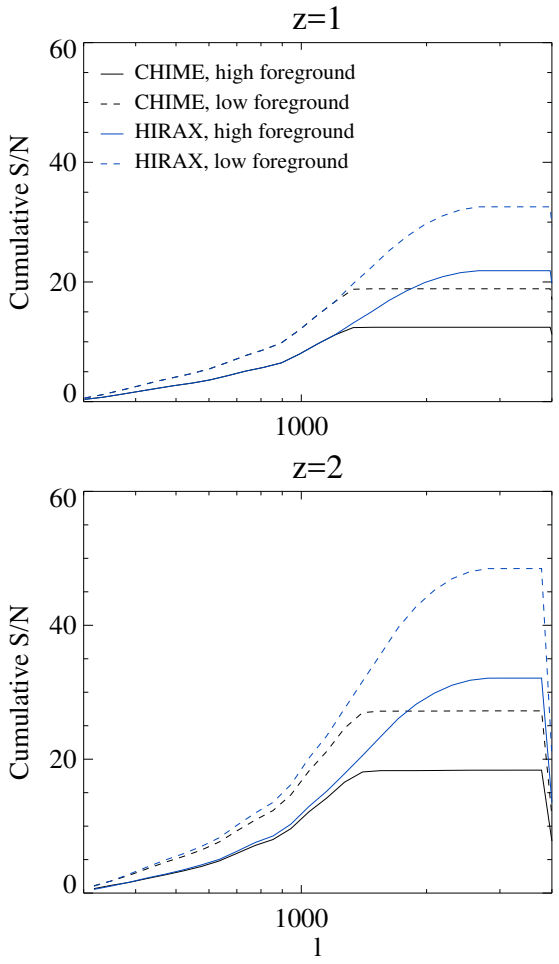

FIG. 5: Cumulative S/N, assuming Planck noise at 217 GHz, $f_{sky} = 0.8$.

Where $C_l^{\rm CMB}$ is the angular powerspectrum of primary CMB ; $C_l^{\rm CMB,N}$ indicates the facility noises; $C_l^{{\rm kSZ},\Delta z}$ is the kSZ signal from a certain redshift bin; r is the correlation coefficients we get; $f_{\rm sky}$ is the percent of sky area covered by both surveys.

In our case, $C_l^{\rm CMB}$ is calculated from CAMB [25]. $C_l^{\rm CMB,N}$ is estimated with Planck results [23] at 217GHz. $C_l^{\rm CMB,N} = (\sigma_{p,T}\theta_{\rm FWHM})^2 W_l^{-2}$; where $\sigma_{p,T} = 8.7\mu K_{\rm CMB}$ is Sensitivity per beam solid angle, $\theta_{\rm FWHM} \sim 5'$ is the effective beam FWHM, $W_l = \exp[-\ell(\ell+1)/2\ell^2_{\rm beam}]$ is the smoothing window function, with $\ell_{\rm beam} = \sqrt{8\ln 2}/\theta_{\rm FWHM}$. We choose $f_{\rm sky} = 0.8$ according to claimed 21 cm intensity mapping survey area. $C_l^{{\rm kSZ},\Delta z}$ is calculated within two bins of size 1200 Mpc/h, centered at redshift 1,2 respectively.

The cumulative S/N is demonstrated in Fig.5. The low correlation in $z = 2$ is compensated by the high electron density and the overall S/N could well reach 50 with HIRAX.

With noise level of Planck, the resolution of HIRAX already cover most important ℓs. However, with $4_{\rm th}$ generation facilities, more detectable modes will apprear in higher ℓs, and better S/N could be expected with longer baselines like SKA.

VIII. CONCLUSION

In this paper, we discuss the possibility of cross correlating kSZ signal with 21 cm intensity mapping to study baryon distributions. All the calculations are based on ongoing experiment condition and realistic noise scales. A holographic way of cross correlation is applied. Second order tidal coupling of different scales are employed to compensate for lost large scale modes. With existing Planck data, it is reasonable to expect at least 15 S/N with data from CHIME, and more optimistic estimates will yield 50 S/N for redshift 2 with HIRAX. The main obstacle for optimal correlation is lack of low k_z high $k_\perp$ data due to foregrounds. This leads to information waste in the reconstructed velocity field. However, data from weak lensing, photo-z galaxy surveys, which contains only large scale structure in z direction, may compensate for that.

This method is promising for its feasibility and model independence. CHIME already starts to collect data, and HIRAX is also in a close flight. It is reasonable to expect it to be tested within five years. Moreover, the method does not rely on assumptions about velocity fields or interstellar medium conditions. Less misunderstanding will appear while interpreting results. It is reasonable to expect it to be a new reliable attemp to study baryon distributions up to redshift 2 or higher. This will foster the understanding of baryonic feedbacks of galaxies, and the study intergalactic medium.

IX. ACKNOWLEDGE

We acknowledge discussions Wenkai Hu, Tianxiang Mao and Jiawei Shao. The simulations were performed on the BGQ supercomputer at the SciNet HPC Consortium. SciNet is funded by: the Canada Foundation for Innovation under the auspices of Compute Canada; the Government of Ontario; the Ontario Research Fund – Research Excellence; and the University of Toronto. Research at the Perimeter Institute is supported by the Government of Canada through Industry Canada and by the Province of Ontario through the Ministry of Research & Innovation. The Dunlap Institute is funded through an endowment established by the David Dunlap family and the University of Toronto.

[1] U.-L. Pen, ApJ **510**, L1 (1999), astro-ph/9811045.
[2] A. M. Sołtan, A&A **460**, 59 (2006), astro-ph/0604465.
[3] R. A. Sunyaev and Y. B. Zeldovich, Comments on Astrophysics and Space Physics **4**, 173 (1972).
[4] R. A. Sunyaev and I. B. Zeldovich, MNRAS **190**, 413 (1980).
[5] E. T. Vishniac, ApJ **322**, 597 (1987).
[6] M. Fukugita and P. J. E. Peebles, ApJ **616**, 643 (2004), astro-ph/0406095.
[7] N. Hand, G. E. Addison, E. Aubourg, N. Battaglia, E. S. Battistelli, D. Bizyaev, J. R. Bond, H. Brewington, J. Brinkmann,

B. R. Brown, et al., Physical Review Letters **109**, 041101 (2012), 1203.4219.

[8] J. Shao, P. Zhang, W. Lin, Y. Jing, and J. Pan, MNRAS **413**, 628 (2011), 1004.1301.

[9] M. Li, R. E. Angulo, S. D. M. White, and J. Jasche, MNRAS **443**, 2311 (2014), 1404.0007.

[10] J. C. Hill, S. Ferraro, N. Battaglia, J. Liu, and D. N. Spergel, ArXiv e-prints (2016), 1603.01608.

[11] S. Ferraro, J. C. Hill, N. Battaglia, J. Liu, and D. N. Spergel, ArXiv e-prints (2016), 1605.02722.

[12] Y. Xu, X. Wang, and X. Chen, ApJ **798**, 40 (2015), 1410.7794.

[13] http://www.acru.ukzn.ac.za/ hirax/.

[14] T. Di Matteo, B. Ciardi, and F. Miniati, MNRAS **355**, 1053 (2004), astro-ph/0402322.

[15] K. W. Masui, E. R. Switzer, N. Banavar, K. Bandura, C. Blake, L.-M. Calin, T.-C. Chang, X. Chen, Y.-C. Li, Y.-W. Liao, et al., ApJ **763**, L20 (2013), 1208.0331.

[16] U.-L. Pen, R. Sheth, J. Harnois-Deraps, X. Chen, and Z. Li, ArXiv e-prints (2012), 1202.5804.

[17] H.-M. Zhu, U.-L. Pen, Y. Yu, X. Er, and X. Chen, ArXiv e-prints (2015), 1511.04680.

[18] E. R. Switzer, T.-C. Chang, K. W. Masui, U.-L. Pen, and T. C. Voytek, ApJ **815**, 51 (2015), 1504.07527.

[19] K. W. Masui, E. R. Switzer, N. Banavar, K. Bandura, C. Blake, L.-M. Calin, T.-C. Chang, X. Chen, Y.-C. Li, Y.-W. Liao, et al., ApJ **763**, L20 (2013), 1208.0331.

[20] E. R. Switzer, K. W. Masui, K. Bandura, L.-M. Calin, T.-C. Chang, X.-L. Chen, Y.-C. Li, Y.-W. Liao, A. Natarajan, U.-L. Pen, et al., MNRAS **434**, L46 (2013), 1304.3712.

[21] J. R. Shaw, K. Sigurdson, M. Sitwell, A. Stebbins, and U.-L. Pen, Phys. Rev. D **91**, 083514 (2015), 1401.2095.

[22] K. Bandura, G. E. Addison, M. Amiri, J. R. Bond, D. Campbell-Wilson, L. Connor, J.-F. Cliche, G. Davis, M. Deng, N. Denman, et al., in *Society of Photo-Optical Instrumentation Engineers (SPIE) Conference Series* (2014), vol. 9145 of *Society of Photo-Optical Instrumentation Engineers (SPIE) Conference Series*, p. 22, 1406.2288.

[23] Planck Collaboration, R. Adam, P. A. R. Ade, N. Aghanim, M. Arnaud, M. Ashdown, J. Aumont, C. Baccigalupi, A. J. Banday, R. B. Barreiro, et al., ArXiv e-prints (2015), 1502.01587.

[24] J. Harnois-Déraps, U.-L. Pen, I. T. Iliev, H. Merz, J. D. Emberson, and V. Desjacques, MNRAS **436**, 540 (2013), 1208.5098.

[25] A. Lewis, A. Challinor, and A. Lasenby, Astrophys. J. **538**, 473 (2000), astro-ph/9911177.